

Article

Wind Waves Web Atlas of the Russian Seas

Stanislav Myslenkov ^{1,2,3,*} , Timofey Samsonov ^{1,3} , Anastasia Shurygina ¹, Sofia Kiseleva ¹
and Victor Arkhipkin ¹ 

- ¹ Department of Oceanology, Faculty of Geography, Lomonosov Moscow State University, GSP-1, Leninskie Gory, 119991 Moscow, Russia; tsamsonov@geogr.msu.ru (T.S.); shur.a17@yandex.ru (A.S.); k_sophia_v@mail.ru (S.K.); victor.arkhipkin@gmail.com (V.A.)
- ² Shirshov Institute of Oceanology, Russian Academy of Sciences, Nakhimovskiy pr. 36, 117997 Moscow, Russia
- ³ Hydrometeorological Research Centre of Russian Federation, Bolshoy Predtechensky Lane, 123376 Moscow, Russia
- * Correspondence: stasocean@gmail.com

Abstract: The main parameters of wind waves in the World Ocean are connected with global climate change. Renewable energy technologies, intensive shipping, fishery, marine infrastructure, and many different human marine activities in the coastal zone and open sea need knowledge about the wind-wave climate. The main motivation of this research is to share various wind wave parameters with high spatial resolution in the coastal zone via a modern cartographic web atlas. The developed atlas contains information on 13 Russian Seas, including the Azov, Black, Baltic, Caspian, White, Barents, Kara, Laptev, East Siberian, Chukchi, Bering Seas, the Sea of Okhotsk, and the Sea of Japan/East Sea. The analysis of wave climate was based on the results of wave modeling by WAVEWATCH III with input NCEP/CFSR wind and ice data. The web atlas was organized using the classic three-tier architecture, which includes a data storage subsystem (database server), a data analysis and publishing subsystem (GIS server), and a web application subsystem that provides a user interface for interacting with data and map services (webserver). The web atlas provides access to the following parameters: mean and maximum significant wave height, wave length and period, wave energy flux, wind speed, and wind power. The developed atlas allows changing the map scale (zoom) for detailed analysis of wave parameters in the coastal zones where the wave model spatial resolution is 300–1000 m.



Citation: Myslenkov, S.; Samsonov, T.; Shurygina, A.; Kiseleva, S.; Arkhipkin, V. Wind Waves Web Atlas of the Russian Seas. *Water* **2023**, *15*, 2036. <https://doi.org/10.3390/w15112036>

Academic Editor: Chin H Wu

Received: 20 April 2023

Revised: 23 May 2023

Accepted: 25 May 2023

Published: 27 May 2023



Copyright: © 2023 by the authors. Licensee MDPI, Basel, Switzerland. This article is an open access article distributed under the terms and conditions of the Creative Commons Attribution (CC BY) license (<https://creativecommons.org/licenses/by/4.0/>).

Keywords: web mapping; web atlas; wind waves; wave modelling; wave energy; wind energy; Russian seas

1. Introduction

Wind wave modeling for long periods helps to understand climate changes on Earth that occurred in the past and to improve their forecast in the future. Coastal and marine infrastructures are most vulnerable during storms, so studying the seasonal and interannual variability of sea storms is important.

Currently, there is quite a lot of interest in estimating the potential of wind and wave energy along the coasts. This is due to the shifting of wind turbine installation sites to the coastal zone, increasing the number of potential consumers of wind and wave energy (autonomous facilities, offshore platforms, lighthouses, communication towers, etc.). There is a general trend of switching from traditional energy sources to alternative ones. The research tasks of developing innovative technologies in the field of wind and wave ocean energy in Russia are outlined in the Maritime Doctrine of the Russian Federation 2022 [1], which is a strategic planning document defining the state policy of our country in the field of maritime activities.

Russia is washed by thirteen seas, and its water border stretches for 40,000 km, so the total energy resources of wind waves in the country are very large. According to

preliminary estimates, the wave energy flux in the Barents Sea can reach the value of 29 kW/m of the wave front and 30–35 kW/m for the ice-free waters of the Sea of Okhotsk and Bering Sea [2,3].

Wind waves are being studied by numerous methods with the use of different sources and approaches around the world, such as direct measurements [4], altimetry use [5], and numerical simulations [6–8]. Direct measurements provide data only for scattered stations for a limited time period. The altimetry data are also spatially limited. Meanwhile, numerical modeling allows obtaining a wide spatiotemporal coverage of different wind wave parameters limited only by the quality of input data.

Regular and extreme characteristics of wind and waves for 10 Russian seas (except the Laptev, East Siberian, and Chukchi Seas) are given in the Wind and Wave Climate Handbooks of the Russian Maritime Register of Shipping [9–12]. These data are based on the results of modeling, but they have to be improved and updated by the last high-resolution atmospheric reanalysis, detailed computational grid, and more modern bathymetry.

There are numerous investigations where the peculiarities of wind waves in the seas of Russia were considered [13–16]. These are usually regional estimates for a specific sea or generalizations for a large region. In these works, as a rule, modern wind reanalysis ERA5 (ECMWF (European Centre for Medium-Range Weather Forecasts) re-analysis v5) and CFSR (Climate Forecast System Reanalysis) were used.

A number of valuable articles were devoted to the Arctic wave climate based on satellite data and simulation results [15–19]. Inter-annual variations of the mean and extreme significant wave height (SWH) in ice-free conditions in the Kara Sea were described by Duan et al. [20]. Some features of the wave parameters in the Barents Sea were presented by Aarnes et al. [21].

Many research papers were devoted to wave modeling in the Black Sea [22–25]. Wave climate of the Caspian Sea based on altimetry and modeling data was presented in [26–30].

WAVEWATCH III (WW3) and Simulating Waves Nearshore (SWAN) models were adopted to forecast wind wave parameters in the Far Eastern Seas and North Pacific [31]. Lyubitskiy et al. [32] described a marine hazard method of the Far Regional Hydrometeorological Research Institute. The wave climate of the Sea of Okhotsk was also considered [33]. Wave parameters of the Sea of Japan/East Sea were investigated by Lee et al. [34] and Sasaki [35]. A high-resolution wave climate hindcast along the Japanese coast was presented by Shimura and Mori [36].

A number of articles were devoted to the Azov, White, and Baltic Seas wave climate based on model results and simulation results [6,12–14,37–41].

To date, the results of such investigations were commonly represented in the form of static maps. For such representation, it is not possible to specify the wave parameters for the coastal zone in fine resolution. Alternatively, if a database is published, special software is required for data visualization. A good alternative example is the APPMAR 1.0 application, which helps to visualize and analyze wind and wave data from databases of the National Oceanic and Atmospheric Administration (NOAA) [42]. However, the resolution of NOAA wave reanalysis is coarse, and the user needs to know Python programming language.

Electronic web atlases are more convenient for users since they provide the ability to select the necessary parameters, area, and map scale. There is an example of such an atlas for the Australian coast [43] and the Black Sea [44]. Atlas of global wave energy based on a rough hindcast ($1.25^\circ \times 1^\circ$ resolution) was presented in [45]. Ireland's Marine Atlas (<https://atlas.marine.ie> accessed on 30 April 2023) is a regional project with high-resolution wind and wave data. Several web services provide wind and wave energy distribution data with rough spatial resolution in the global World Ocean or local regions [46–51]. Atlas of renewable energy sources for the territory of Russia (<http://gisre.ru/> accessed on 30 April 2023) allows the user to evaluate the potential of solar or wind energy [52].

However, it is very difficult to find the necessary information about the parameters of wind waves for a particular sea. It is even more complicated if the user needs information in high spatial resolution near the shore. Preliminary results about the content and technical

parameters of wind waves web atlas of the Russian Seas were published in [53,54]. The current paper provides a more detailed and extended analysis alongside the presentation of the final product.

The main goal of the current research was to develop a special web atlas that allows users to get wind wave information in open access (<https://carto.geogr.msu.ru/wavenergy/>; <http://93.180.9.222/wavenergy> accessed on 30 April 2023) for 13 seas washing Russia, including the Azov, Black, Baltic, Caspian, White, Barents, Kara, Laptev, East Siberian, Chukchi, Bering Seas, the Sea of Okhotsk and the Sea of Japan/East Sea. We used modern, high-quality reanalysis of wind and ice data, the WW3 model, and detailed bathymetry on a high-resolution unstructured mesh (up to 300 m). Modern web mapping technologies were applied to deliver cartographic presentations of the modeled parameters. The following paper chapters describe the methodological and technological foundations of the atlas in more detail.

2. Data and Methods

2.1. Wave Model Description and Configuration

The main data displayed in the web atlas was obtained based on the WW3 6.07 spectral wave model [55]. This state-of-the-art model is widely applied for reconstructing wave fields [7,19]. The WW3 model considers wind speed, ice concentration, and physical effects described below. A numerical solution of the wave action density spectrum equation is based on:

$$\frac{DN}{Dt} = \frac{S}{\sigma}, \quad (1)$$

where $N(k, \theta) \equiv F(k, \theta)/\sigma$, k —wavenumber, θ —propagation direction, σ —relative frequency, D/Dt represents the total derivative (moving with a wave component) and S represents the net effect of sources and sinks for the surface elevation variance density spectrum F [55]. S is a source function that describes the energy transfer from the wind to the waves, nonlinear wave interactions, and energy dissipation through the collapse of the crests at a great depth and in the coastal zone, friction against the bottom and ice, wave scattering by ground relief forms, and reflection from the coastline and floating objects. The energy balance equation is integrated using finite-difference schemes by the geographic grid and the wave parameters spectrum.

In this study, the calculations were made using the ST6 physics package [56,57]. The ST6 physics describes wind–wave exchange, based on experimental and theoretical research [56]. A discrete interaction approximation model was used for the possible nonlinear interactions of the waves. The approach of Battjes and Janssen (1978) was adopted for the wave height growth with the depth decrease in shallow water and for the related wave breaking with critical steepness value. The standard Joint North Sea Wave Observation Project (JONSWAP) scheme was applied for bottom friction. The model spectral resolution is 36 directions (10°), and the frequency range includes 36 intervals from 0.03 to 0.843 Hz. The time step for the integration of the complete wave action equation was set to 15 min. The time increment for the integration of the functions of the wave energy sources and sinks was 60 s, and the time increment for the spectral energy transfer was 450 s.

The influence of sea ice on the waves was calculated via the IC0 scheme. A grid point was considered ice-covered when the ice concentration was >0.5 . We used the basic IC0 scheme since it gives acceptable results (see Section 2.2). We carried out several tests of various ice patterns for the Barents Sea previously and found that the quality of the wave modeling, in general, is independent regardless of the ice scheme choice. Differences were observed only in a narrow strip of ~ 50 km near the ice edge.

A more detailed description of the model configuration and the main results of the experiments with different meshes and computational schemes were presented in [58–60].

Wave model input data of the wind speed at 10 m above the ground and the sea ice concentration were taken from the Climate Forecast System Reanalysis of the National

Centers for Environmental Prediction (NCEP/CFSR) from 1979 to 2010. This reanalysis has a spatial resolution of $0.3^\circ \times 0.3^\circ$ and a time step of 1 h [61]. Starting from 2011, we used NCEP/CFSv2 [62], which is the extension of the previous reanalysis version. It has a more detailed spatial resolution of $\sim 0.205^\circ \times 0.204^\circ$ and the same time step of one hour. The NCEP/CFSv2 sea ice component includes a dynamic/thermodynamic sea ice model and a simple assimilation scheme, which Saha et al. described in detail [61]. The wind speed at the 1000 hPa (~ 110 m) and 975 hPa (~ 300 m) with spatial resolution 0.5° and time step 6 h were taken from NCEP/CFSR to calculate wind power density.

Wave simulations were performed using several unstructured grids for all studied seas (Figure 1). The spatial resolution was 10–20 km in the central open areas of the seas and 300–1000 m in the coastal zones. We used seven computational domains, which are characterized in Table 1. The unstructured grid for the Barents and Kara Seas included the North Atlantic region and the North Pacific for the Far East Seas (Figure 1). This unstructured mesh allowed a high spatial resolution not only in coastal zones but also in the narrow straits. Wave energy can freely pass from the Pacific Ocean through the straits of the Kuril chain and the Aleutian Islands when an unstructured mesh is used. The computational grids were created on the basis of the General Bathymetric Chart of the Oceans 2019 (GEBCO, <https://www.gebco.net/> accessed on 30 April 2023). The bathymetry data were updated for coastal zones by digitized navigation maps with a spatial resolution of 200–300 m. The study of wind waves using an unstructured computational grid is widely used by scientists: the main features of modeling and quality assessments were given in the several works [6,63–65].

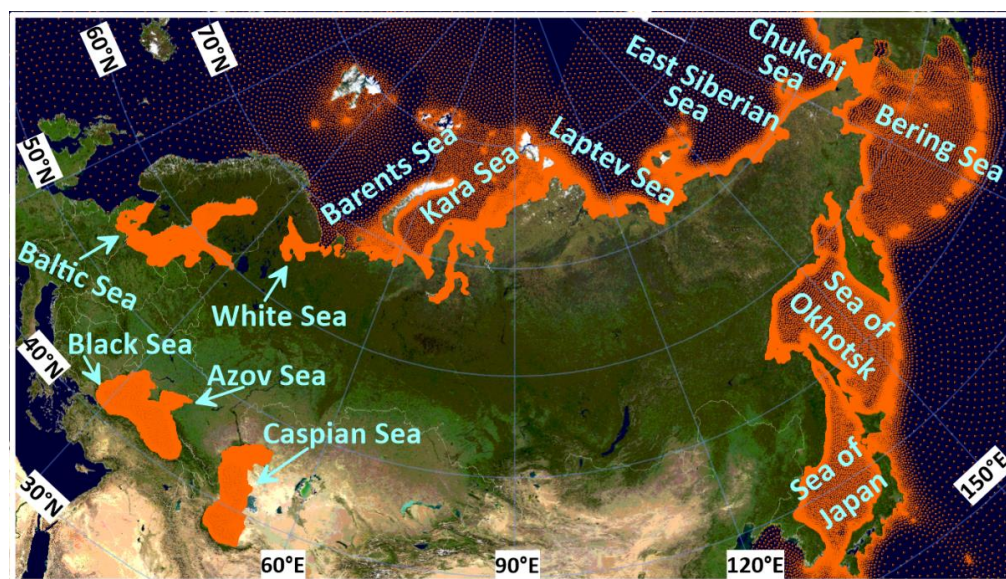


Figure 1. The computational unstructured grids for all researched seas.

Table 1. Basic information about computational domains.

Computational Domain	Included Seas	Total Number of Grid Points	Spatial Resolution in Coastal Zone	Spatial Resolution in Open Sea	Features
1. West Russian Arctic	Kara, Barents	37,729	~700 m	10–20 km	North Atlantic included
2. East Russian Arctic	Laptev, East Siberian, Chukchi	36,176	~800 m	10–15 km	Arctic ocean up to N87 and Beaufort sea included
3. Far-Eastern Russian	Bering, Okhotsk, Japan	69,333	~1000 m	15–25 km	North Pacific included
4.	Black, Azov	59,690	~300 m	5–10 km	
5.	Caspian	17,529	~800 m	10 km	
6	Baltic	34,985	~400 m	10 km	
7.	White	26,587	~400 m	10 km	Barents Sea included

We used only calm wave conditions on the open boundary. Sensitivity tests showed that the open boundary in the central part of the Atlantic Ocean does not influence the waves in the Barents Sea [66]. There is an open boundary in the north for the Barents and Kara Seas, but the sea ice is there almost all the time [59]. The open boundary between the Vilkitsky Strait and the Bering Strait does not greatly influence on the wave statistics.

2.2. Model Quality Assessment

To assess model quality, we used buoy and satellite SWH data. Our previous investigations have shown the high-quality validation for the Kara Sea [59], the Barents Sea [58,67], the Caspian Sea [68] and the Black Sea [69] (Table 2). Generalized statistics were provided for the Laptev, East Siberian, and Chukchi Seas [70], and for the Bering Sea, modeled and measured data were compared using NOAA station (57°0′56″ N, 177°42′11″ W) for the 2018 to 2019 period [60].

Table 2. Basic model quality statistics.

Sea	R	Bias (m)	RMSE (m)	SI (Scatter Index)	N (Total Number)	Reference
Kara	0.89–0.93	−0.03–0.14	0.32–0.38	0.24–0.28	~190,000	Cryosat, Sentinel, Saral [59]
Kara	0.94	0.07	0.32	0.28	400	Buoy data [59]
Barents	0.88	0.04	0.53	0.28	~266,000	CryoSat [67]
Black	0.85	−0.11	0.36	0.36	~61,000	Saral [69]
Black	0.76	−0.11	0.39	0.65	~10,000	Buoy data [69]
Caspian	0.91	0.07	0.29	0.29	~35,000	Saral [68]
Bering	0.97	0.17	0.46	0.12	~4500	Buoy data [60]
Laptev, East Siberian, Chukchi	0.89	−0.05	0.32	0.25	~79,000	CFOSAT [70]

The model quality assessments was based on the standard statistical parameters:

$$\text{Bias} = \sum_{i=1}^N \frac{1}{N} (P_i - O_i), \quad (2)$$

$$\text{RMSE} = \sqrt{\frac{1}{N-1} \sum_{i=1}^N (P_i - O_i)^2}, \quad (3)$$

$$\text{SI} = \frac{\text{RMSE}}{\frac{1}{N} \sum_{i=1}^N O_i}, \quad (4)$$

$$R = \frac{\sum_{i=1}^N ((P_i - P)(O_i - O))}{\sqrt{\left(\sum_{i=1}^N (P_i - P)^2\right) \left(\sum_{i=1}^N (O_i - O)^2\right)}}, \quad (5)$$

where, N is the total number of data, P_i is the model value, O_i is the observed value, P is the mean model value, O is the mean observed value.

The results of quality assessments based on the satellite data and buoy measurements, presented in Table 2, show good model quality which is similar to assessments conducted by other scientists [16,17,19]. Hence, the results allow us to use our web Atlas for fundamental and applied studies.

The wind wave fields, as a model output, were obtained every three hours from 1979 to 2019 (41 years in total) for the Barents, Kara, Bering, Okhotsk, and Japan/East Sea and from 1979 to 2020 (42 years in total) for the Black and Caspian Seas. In this study, only modeled *SWH* results are discussed. We considered *SWH* (m) as $(4\sqrt{m_0})$, where m_0 is the zero-order moment of the wave spectrum. *SWH* is somewhat of the mean value of 1/3 of the highest waves. The analyzed statistical parameters were the 95% percentile *SWH*, long-term maximum, and mean *SWH*. Maximum *SWH* is the highest *SWH* for the whole modeled period for each point. If the sea surface was ice covered, the *SWH* in this node was equal to zero. The mean long-term characteristics include it in calculations as zero data.

2.3. Spatial Data Models and Processing

Wave and wind modeling results should be represented via spatial data models, which can be processed by Geographic Information System (GIS) software and visualized using web mapping libraries. This transformation requires the selection of optimal data models and programming of the technological transition between the source and the spatial data. The main requirement of such a transition is to minimize the error of representation—i.e., GIS representation should reflect the modeling data as accurately as possible. The second requirement is the ability to visualize the resulting data in a cartographic form: isolines for wave parameters and a choropleth map for wind parameters. The third and the final requirement is the ability to perform spatial queries of wave and wind parameters, i.e., the user should be able to fetch the value at any specified point.

2.3.1. Wave Parameters

The WW3 model used to calculate the wave parameters operates on the irregular triangulation grid. This spatial layout corresponds naturally to the Triangulated Irregular Network (TIN) spatial data model [71], handled by spatial database management systems (DMBSs) and desktop GIS software. However, visualization of TIN is not supported by modern Open Geospatial Consortium (OGC) web service standards (WMS, WFS), as well as data visualization software libraries (such as OpenLayers and Leaflet). Therefore, this data cannot be directly used in web atlas and must be transformed into another spatial data model, such as a raster or vector model.

The most straightforward alternative to TIN is a raster spatial data model. Both are coverage models [72] used for the representation of continuous fields, but the raster is constrained by regular sampling along axes. Therefore, if the raster model is utilized, the main question is to decide on the optimal resolution. Data loss can be avoided if the sampling frequency is twice larger than the spatial frequency—the Nyquist frequency [73]. By interpreting this statement in the context of the raster model we can say that the resolution of the raster should be at least two times higher than the minimum distance

to the nearest neighbor in the analyzed set of wave modeling points. The calculations show that a resolution of 300 m is sufficient for the computational grid over the Black Sea. This resolution would result in a raster that has 6000×3600 size, or 21.6 million nodes. However, according to Table 1, the Black and Azov Seas model contains only ~59,690 nodes. Hence, the raster data structure is exceedingly ineffective for GIS representation of the results.

Since the required cartographic representation of wave parameters is isolinear, we ended with a compromised solution based on a combination of two spatial data models: TIN and vector. First, the triangulated surface was reconstructed from the coordinates of the modeling grid. This results in a TIN data structure identical to the one used by the WW3 model. Second, three vector outputs were generated from the TIN: isolines, isobands, and the Voronoy diagram.

Isolines and isobands (polygons between isolines) were used for the cartographic representation of the wave parameters, where isobands are colored and isolines are labeled. Isolines were extracted with value step specific for each wave parameter and using linear interpolation on the TIN faces. When linear interpolation is used, the surface within each triangle is represented as a piece of the plane that passes through its points. This leads to contours that are straight linear segments inside each triangle and can be extracted very quickly.

The Voronoy diagram was used for spatial queries. A Voronoy diagram of a finite set of points S in the plane represents a partition of the plane in which each region of that partition forms a set of points closer to one of the elements of the set S than to any other element of the set. Representation of the Voronoy diagram as a set of spatial polygons provided a vector coverage of the modeling area from which the value can be sampled at any point.

Thus, all three requirements of GIS representation of wave parameters were satisfied. TIN data model allowed lossless representation of the source data. Isolines/isobands were used for cartographic representation. And the Voronoy diagram feeds spatial queries. These data were organized as layers in a spatial database—one for each wave parameter.

2.3.2. Wind Power Density Parameters

Data on wind energy in the coastal region are a sparse set of regularly arranged points with a step of 0.5° , distributed in the form of a narrow strip along the coastline. In this case, interpolation of the surface by methods that ensure the continuity of the distribution is impractical due to the limited number of modeling points and the elongated configuration. At the same time, it is desirable to create a continuous coverage of coastal areas to ensure effective cartographic representation.

The nearest neighbor (NN) interpolation method was considered a compromise option. Each point within the interpolation area receives the value from the point of the source data closest to it. As a result, a stepped surface is obtained, covering the interpolation area in a continuous manner. Technologically this approach was implemented by constructing a Voronoy diagram for a set of source data points. Since the points were arranged in a lan/lot grid, the resulting Voronoy diagram is represented by a set of quadrangles. Each quadrangle can be visualized using the choropleth approach, i.e., by applying the fill color that corresponds to the value.

To limit the area of the Voronoi diagram construction, the centerline of the set of points was manually constructed. Then the centerline is buffered so that the resulting buffer zone covers the original set of points with a margin equal to the average distance between the points. The calculations performed for the initial set of points give a buffer radius of 50 km.

Furthermore, we also satisfied the three initial requirements in the case of wind power density parameters. Voronoy polygons have a one-to-one relationship with the source data; hence the transformation between data models is lossless. Second and third, Voronoy polygons were used for cartographic representation and spatial queries.

2.3.3. Data Integration

Since the modeling was performed independently for each sea, the problem of data integration arose for all neighboring seas. To obtain a seamless GIS data coverage for each wave and wind parameter, an intermediate step was introduced into processing. First, the modeling points for all seas were merged into one TIN. Then this TIN was edited to remove possible edge effects in areas where modeling domains coincide. In the case of wind parameters, the editing was performed in automatic mode by averaging the overlapping values. Finally, the resulting surface was used to construct the isolines/isobands and the Voronoy diagram.

2.4. Technological Architecture of the Atlas

The source data grid is presented in the geographical coordinate system WGS 84 (EPSG code is 4326). For the cartographic visualization and interpolation of data, it was projected into a flat rectangular coordinate system—Web Mercator/Pseudo Mercator (EPSG code is 3857) commonly used in web services. The parameters of wave and wind energy were shown by isolines and isobands (layered coloring). The color scales of unipolar and bipolar indicators were developed based on the Color Brewer color palette system.

The overall architecture of the web atlas was based on a three-tier model, which includes a data storage subsystem (database server), a data analysis and publication subsystem (GIS server), and a web application subsystem that provides a user interface for interacting with data and mapping services (web server). The architecture of the web atlas is shown in Figure 2. The choice of the subsystem distribution scheme for computing units (physical servers) depends on the potential load on the system and the involvement of subsystems in solving other tasks. The current assessment of the potential user load (no more than a few dozen people at any given time) and the relative simplicity of the database and mapping services made it possible to implement the placement of all three subsystems on one physical server. The data is transferred from server to client using a Web feature service (WFS) OGC protocol.

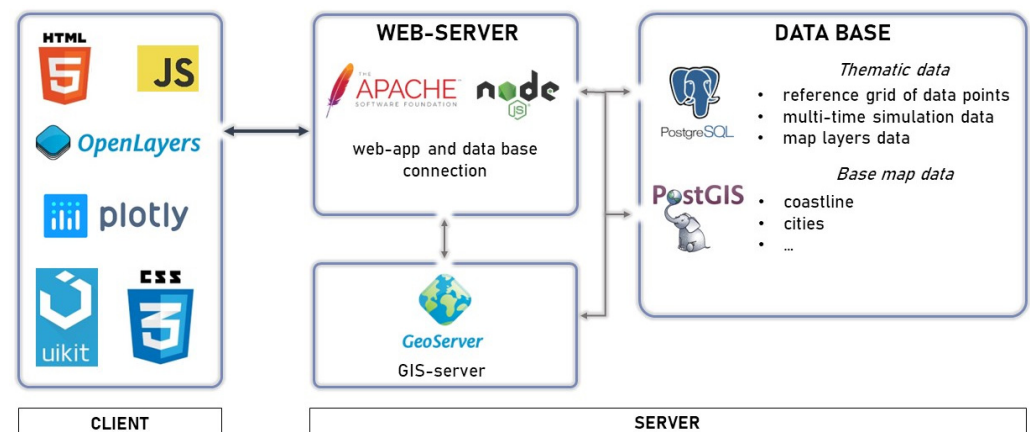


Figure 2. Web atlas architecture and technologies.

3. Results and Discussion

In the first part of this chapter, we present the main functions of web atlas with interface examples. In the second part, the main advantages of web atlas are discussed. In the third part, the comparison of our wave calculations with the other models and the effect of using the unstructured grid in wave modeling is presented.

3.1. Web-Atlas Main Functions

The web atlas is located at <https://carto.geogr.msu.ru/wavenergy/> (or the development version at <http://93.180.9.222/wavenergy> accessed on 30 April 2023). The starting page presents the distribution of the maximum significant wave height in the seas under

study (Figure 3). In the upper left corner, there is a Layers button for switching layers. By switching layers, the user has the opportunity to choose one of the following parameters:

- maximum significant wave height, m;
- maximum wave height (1% probability of exceedance), m;
- mean significant wave height, m;
- maximum wave energy flux, kW/m;
- mean wave energy flux, kW/m;
- mean wave length, m;
- mean wave period T01, s;
- probability of wave energy > 1 kW/m, %;
- mean wind power density 50 m above the ground, W/m²;
- mean wind power density 100 m above the ground, W/m²;
- mean wind speed 50 m above the ground, m/s;
- mean wind speed 100 m above the ground, m/s.

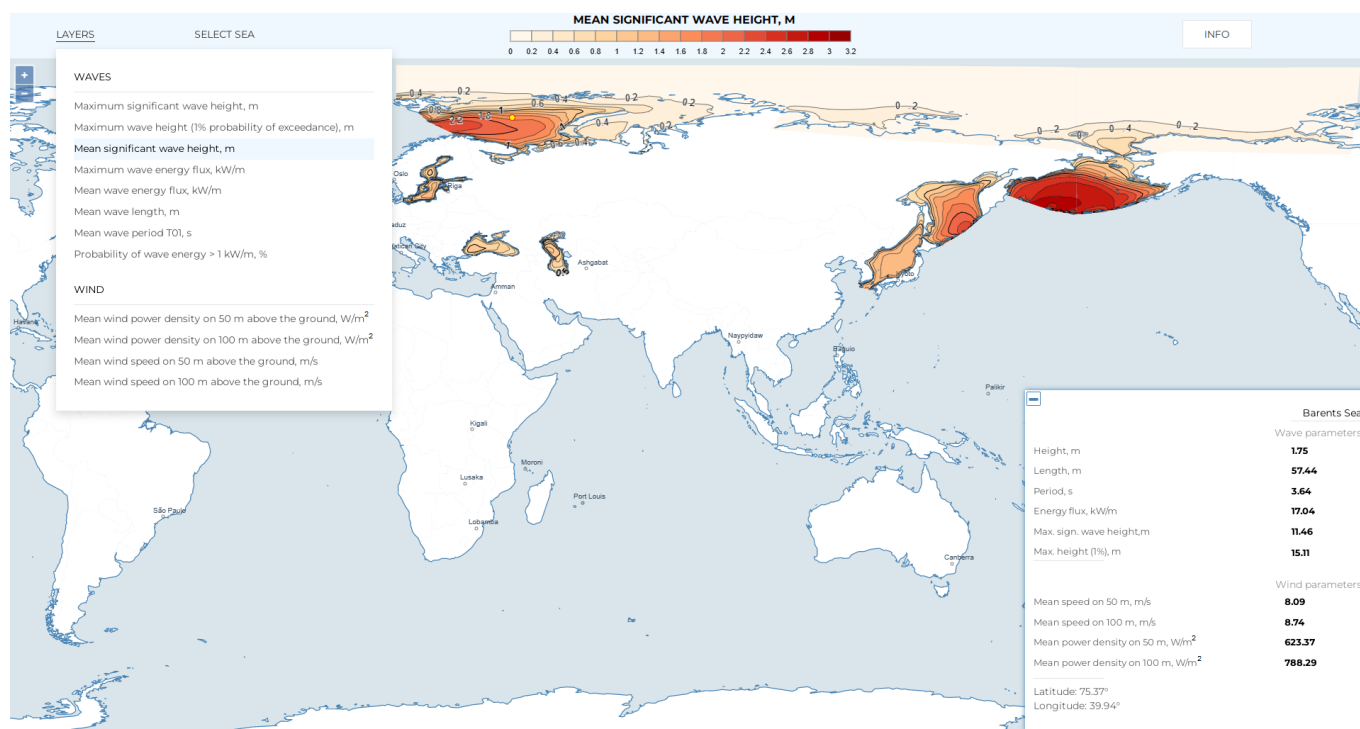


Figure 3. Web atlas overview with “mean significant wave height” parameter selected. The yellow dot shows the selected point for analysis.

The user can use the mouse, touch bar, or screen to pan and zoom the map. There is a button for selecting a specific sea, which makes it easier to find the water area. If the user chooses the specific sea, the map zooms to its extent, and changing the parameter is followed by changing the represented map. An example of the maximum significant wave height in the Laptev, East Siberian, Chukchi, Bering, Okhotsk, and East/Japan Seas is represented in Figure 4.

When left-clicking on any point located within the explored seas, the user receives a table of values, presented in the lower right corner (Figure 3). For the selected point, the coordinates and all the main wave and wind parameters are displayed.

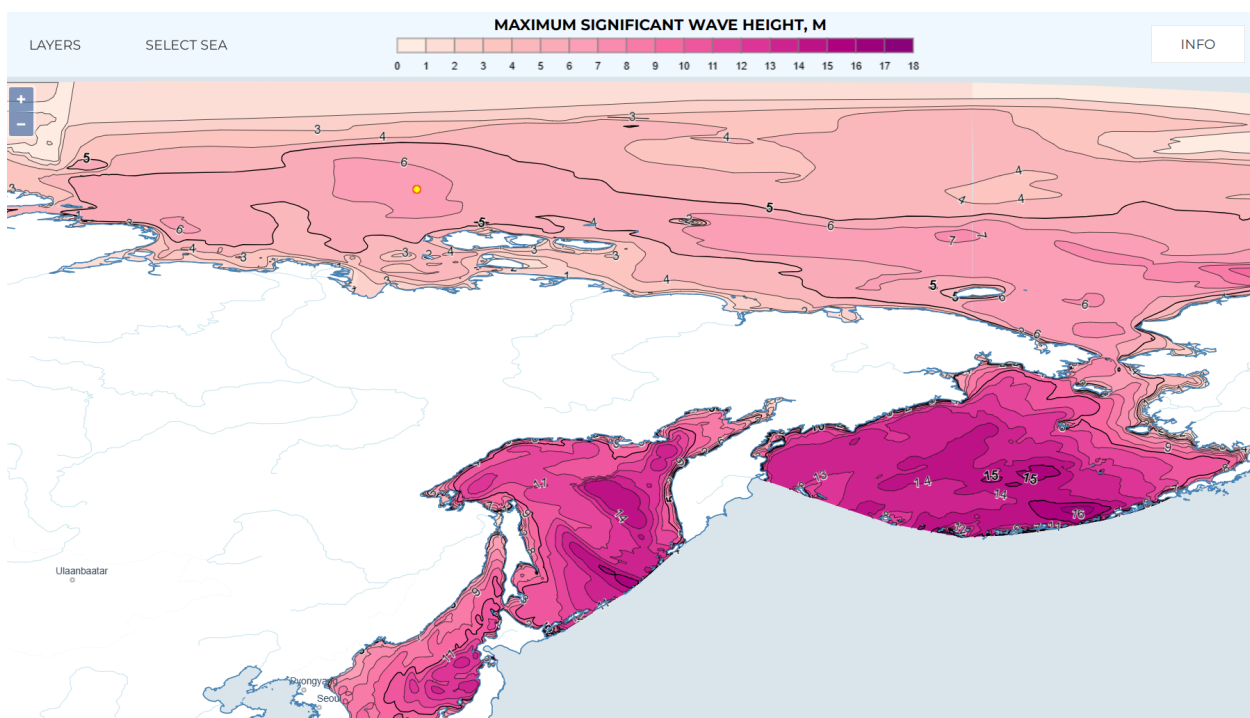


Figure 4. Maximum significant wave height in the Laptev, East Siberian, Chukchi, Bering, Okhotsk and East/Japan Seas displayed in the web atlas.

3.2. The Main Advantages of the Web Atlas

The most important advantage of the developed atlas is the ability to analyze the parameters of waves and wind in 13 seas simultaneously and in high spatial detail. There is no need to search for different data sources. It is possible to analyze wind wave climate, and available energy sources, to reveal the potential places of coastal destruction and other processes that are influenced by wind and waves. The atlas has the ability to dynamically update maps while zooming according to the level of detail. This function allows for the study of sea energy characteristics in different scales. The color fill, isolines, and labels are dynamically rerendered while zooming.

The web atlas was built on modeling data with a high resolution in the coastal zone. This is an outstanding feature since ERA5 databases are presented on a regular grid (e.g., 0.5°), which does not allow the estimation of the distribution of wave parameters near the shore. Usually, modeling data with high resolution are either not published in the public domain or downloaded as large arrays of source data. Our atlas provides access to such data, and we can see its effect on the distribution of maximum significant wave height in the Korean strait, where Tsushima and other islands are correctly represented in the calculated grid (Figure 5). It is seen that the islands influence the propagation of wave energy significantly, which proves that calculations using unstructured computational grids are capable of handling the local effects with high accuracy.

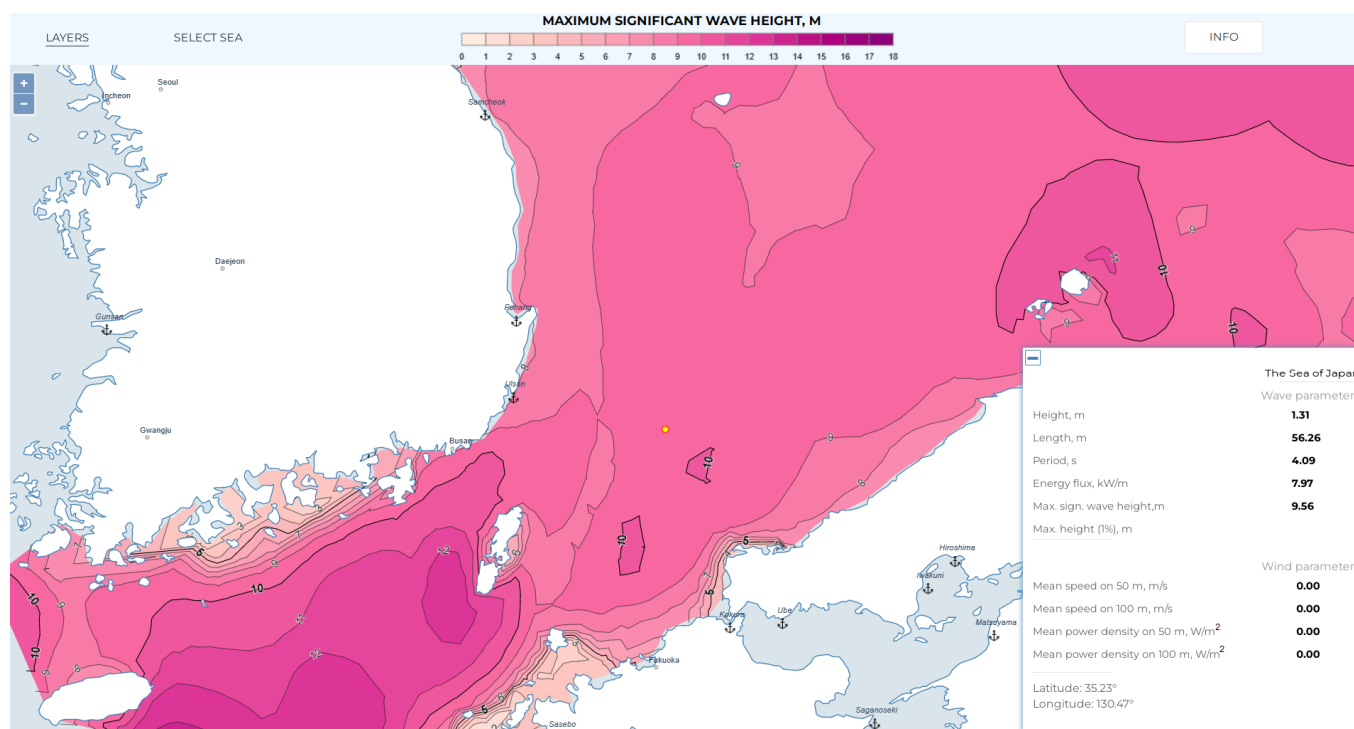


Figure 5. Maximum significant wave height in the Korean strait displayed in the Web atlas. The yellow dot shows the selected point for analysis.

3.3. Comparison of WW3 Unstructured Data with Other Sources

An example of comparing our wave reanalysis which is used for the web atlas, with several popular wave reanalyses in the Bering Sea is shown in Figure 6. We compared the WW3 NOAA dataset (<https://polar.ncep.noaa.gov/waves> accessed on 30 April 2023), which is distributed by Asia-Pacific Data-Research Center (<http://apdrc.soest.hawaii.edu/> accessed on 30 April 2023) (Figure 6a), with the popular wave reanalysis ERA5 [74] (<https://www.ecmwf.int/en/forecasts/dataset/ecmwf-reanalysis-v5> accessed on 30 April 2023) (Figure 6b). Both reanalyses have a spatial resolution of 0.5° . WW3 NOAA was forced by NCEP wind, ERA5 used its own ERA5 wind, and our calculations used NCEP wind and an unstructured grid.

In general, wave height fields based on the different datasets look similar (Figure 6). In this case, the waves come from the Pacific Ocean to the north and pass through the straits of the Aleutian Islands. The width of some straits is less than the resolution of 0.5° , so in the case of a high-resolution unstructured grid, more wave energy passes through the straits to the Bering Sea (Figure 6c).

More detailed wave fields in the Aleutian Islands area are shown in Figure 7. We see that depending on the grid resolution and size of the islands, the wave fields have different features.

The general quality estimates of our implementation (Section 2.2) are comparable to the quality of other reanalyses [19,75,76]. Next, we decided to assess the quality of our wave model implementation based on an unstructured grid using direct wave measurements. Unfortunately, good wave data series are quite rare, especially near straits and islands. We used NOAA wave buoy №46072 (https://www.ndbc.noaa.gov/station_page.php?station=46072 accessed on 30 April 2023), which was located to the south of the Aleutian Islands (Figure 8). When using an unstructured grid, even through narrow straits, wave energy passes freely, which cannot be achieved when using a regular 0.5° resolution grid (Figure 8b).

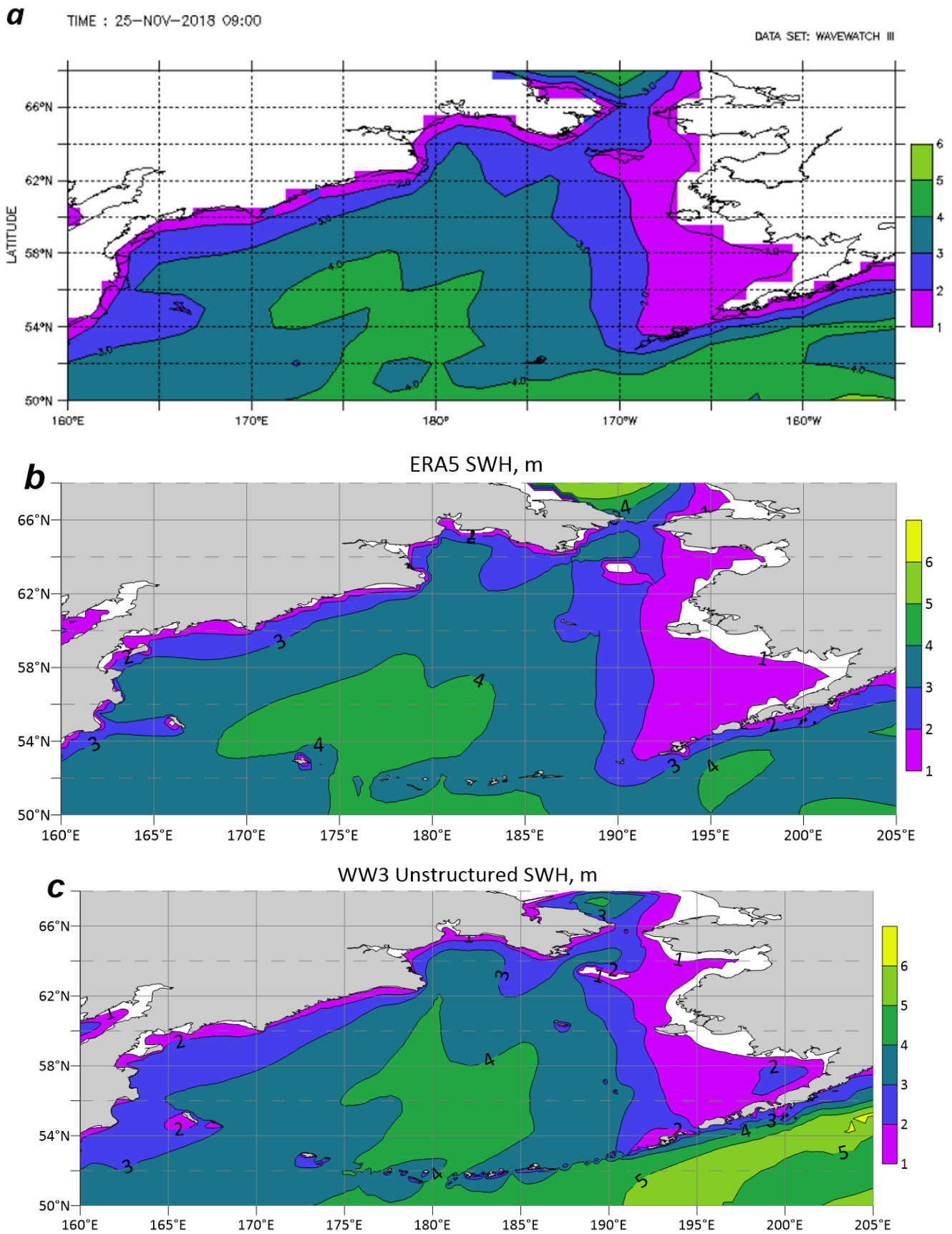


Figure 6. Significant wave height in the Bering Sea at 25.11.2018 based on WW3 NOAA (a), ERA5 (b) and our wave reanalysis (c). Black box used for zoomed in region shown in Figure 7.

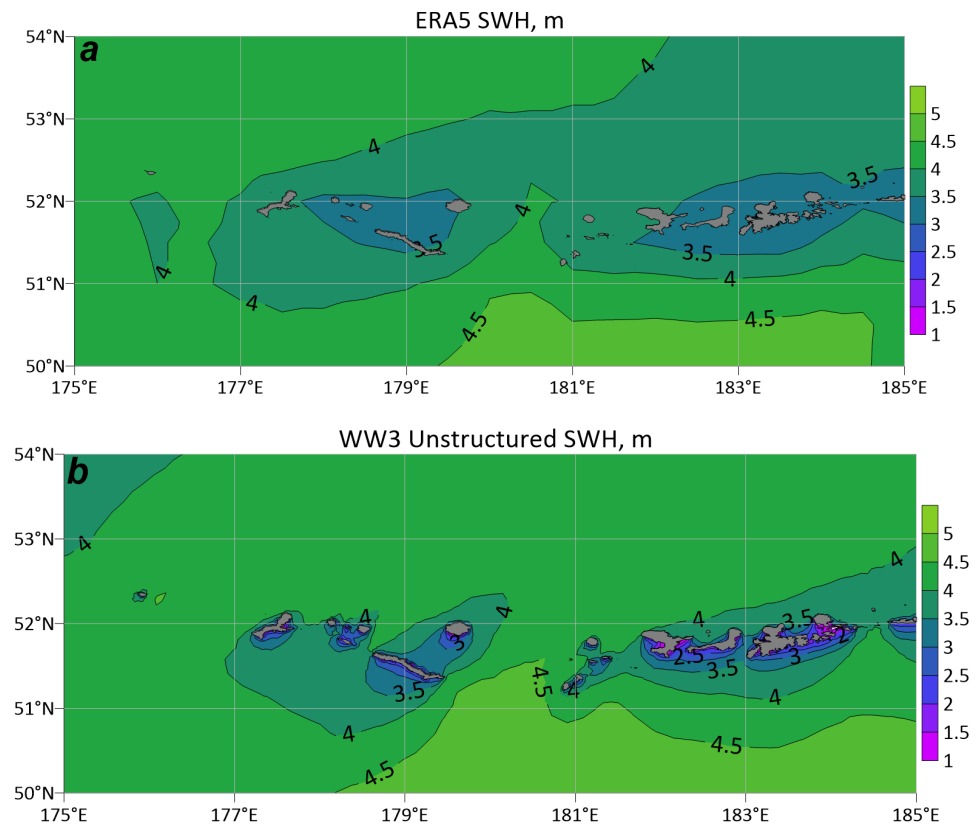


Figure 7. Significant wave height in the selected square of the Aleutian Islands 25 November 2018 based ERA5 (a) and our wave reanalysis (b).

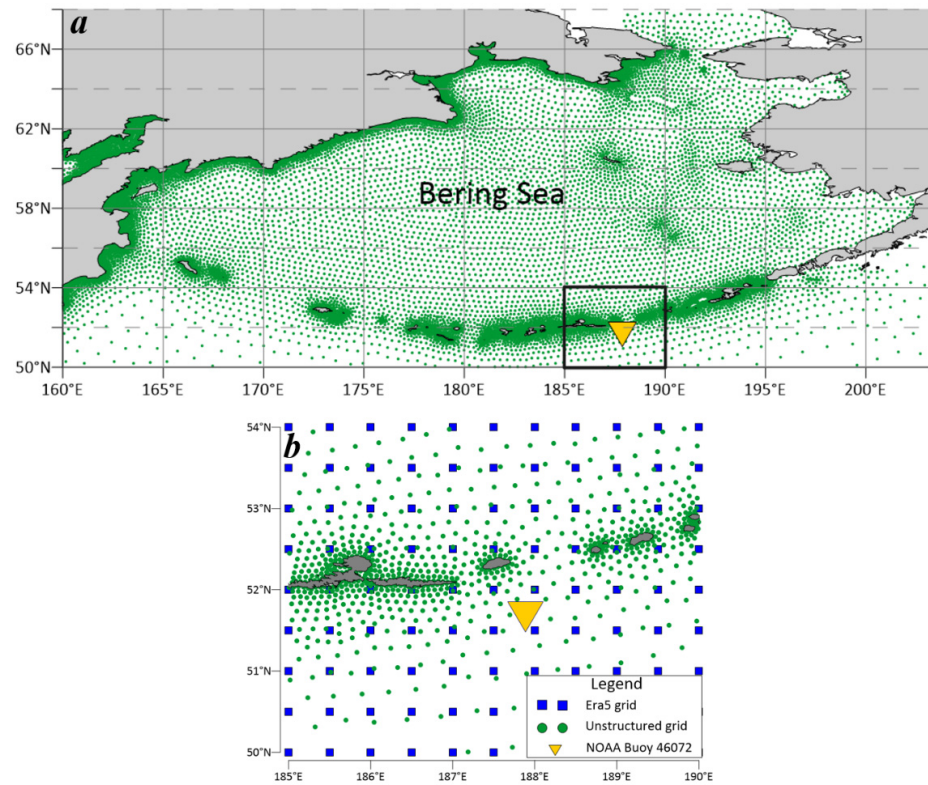


Figure 8. Unstructured grid in the Bering Sea (a), ERA5 and WW3 Unstructured grid in selected square (black box on Figure 8a) of the Aleutian Islands (b).

A comparison of the modeled and measured SWH from 1 November to 1 December 2018 for wave buoy №46072 is shown in Figure 9. Both variants of model calculations (ERA5 and WW3 Unstructured) represent the absolute wave height and the phase of the individual storm event quite well. However, in some cases, there is a difference of about 0.5–1 m between the models. It is important to note that different forcing was used in the wave models, and it is not quite correct to make a direct comparison. We found several cases (highlighted in red circles in Figure 9) when the wave height according to the ERA5 model is lower than the buoy and the WW3 unstructured model. These situations were observed in the direction of waves 250–320° (Figure 9b); hence the waves come from the islands (Figure 8b). The number of nodes in the 250–320° sector in the ERA5 model is insufficient for the correct propagation of wave energy from this direction (Figure 8b). We believe this is to the cause of the underestimation of the height of the waves in the ERA5 model.

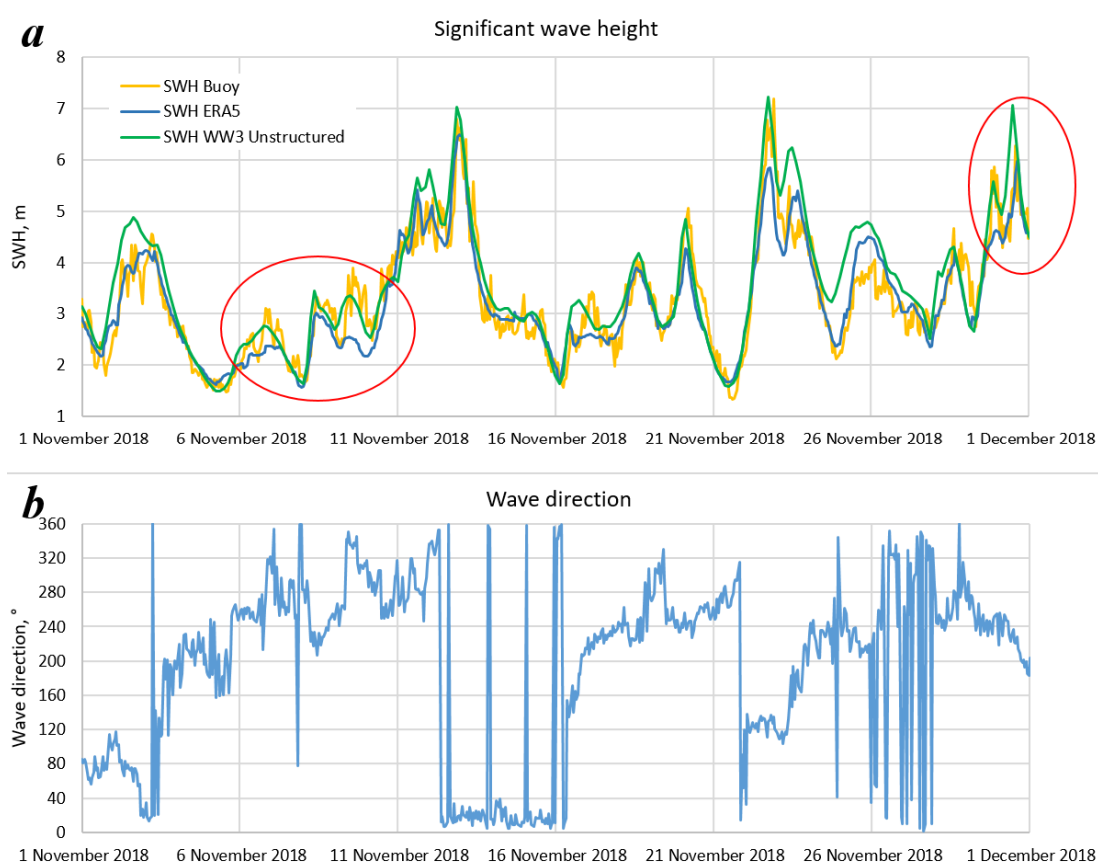


Figure 9. Significant wave height based on buoy measurements, ERA5 and our wave hindcast (a) and mean wave direction based on buoy measurements (b). The red circles show the possible influence of the computational grid.

4. Conclusions

This paper presented the wind waves web atlas of the Russian Seas. The source data, processing, as well as the functionality and characteristics of the atlas were described. The atlas contains the following parameters: mean and maximum values of the significant wave height, wave length and period, wave energy flux, wind speed, and wind power. Spatial distributions of these parameters were obtained through long-term modeling using the WW3 model on an unstructured grid. Technically, the atlas is based on the classic three-tier architecture, which includes a data storage subsystem, data analysis, and publishing subsystems.

The main advantage of the developed atlas is open access—it can be used via a web interface without any special programs and skills. The second important advantage is the ability to change the map scale (zoom) and a detailed analysis of wave parameters in the coastal zones where the wave model spatial resolution is 300–1000 m. Moreover, the use of an unstructured high-resolution grid improved the quality of wave modeling in conditions of a complex coastline and the presence of islands.

This web atlas can be very useful for assessing extreme wave conditions near the coast and the available potential of wave and wind energy in the Russian Seas.

Author Contributions: The concept of the study was developed by S.M. and T.S., S.M. and V.A. did numerical simulations and manuscript writing. A.S. did the data visualization and manuscript writing. S.K. did the manuscript writing. S.M. prepared the paper with contributions from T.S., A.S., S.K., V.A. All authors have read and agreed to the published version of the manuscript.

Funding: This research was funded by the Russian Science Foundation, research project 23-27-00239.

Data Availability Statement: The wind wave statistical information which presented in this article provided in open access (<https://carto.geogr.msu.ru/wavenergy/>; <http://93.180.9.222/wavenergy>). The raw data of the wave calculations are not available in open access.

Conflicts of Interest: The authors declare that the research was conducted in the absence of any commercial or financial relationship that could be considered a potential conflict of interest.

References

1. Maritime Doctrine of Russian Federation. 2022. Available online: <https://maritimeindia.org/maritime-doctrine-of-the-russian-federation-2022-an-analysis-maritime-doctrine-of-the-russian-federation-2022-an-analysis/> (accessed on 18 April 2023).
2. Minin, V.A.; Dmitriev, G.S. *Prospects for Development of Non-Traditional and Renewable Energy Sources on the Kola Peninsula (Perspektivy Osvoeniya Netraditsionnykh i Vozobnovlyаемykh Istochnikov Ehnergii na Kol'skom Poluostrove)*; Bellona Publishing House: Murmansk, Russia, 2007; pp. 58–67. (In Russian)
3. Gorlov, A.A. Scientific and experimental infrastructure of the development of marine Renewable energy. *Energiya Ekon. Tekhnika Ekol.* **2017**, *4*, 21–31. (In Russian)
4. Divinsky, B.V.; Kuklev, S.B. Experiment of Wind Wave Parameter Research on the Black Sea Shelf. *Oceanology* **2022**, *62*, 8–12. [[CrossRef](#)]
5. Young, I.; Ribal, A. Multiplatform evaluation of global trends in wind speed and wave height. *Science* **2019**, *364*, 548–552. [[CrossRef](#)]
6. Amarouche, K.; Akpınar, A.; Soran, M.B.; Myslenkov, S.; Majidi, A.G.; Kankal, M.; Arkhipkin, V. Spatial calibration of an unstructured SWAN model forced with CFSR and ERA5 winds for the Black and Azov Seas. *Appl. Ocean. Res.* **2021**, *117*, 102962. [[CrossRef](#)]
7. Cavaleri, L.; Alves, J.H.; Ardhuin, F.; Babanin, A.; Banner, M.; Belibassakis, K.; WISE Group. Wave modelling—The state of the art. *Prog. Oceanogr.* **2007**, *75*, 603–674. [[CrossRef](#)]
8. Rusu, L.; de León, S.; Soares, C. Numerical modeling of the North Atlantic storms affecting the West Iberian coast. In *Maritime Technology and Engineering*; CRC Press, Taylor & Francis Group: Abingdon, UK, 2015; Volume 2, pp. 1365–1370.
9. Lopatukhin, L.; Buhanovskij, A.; Degtyarev, A.; Rozhkov, V. *Reference Data of Wind and Waves Climate of the Barents, Okhotsk, and Caspian Seas*; Russian Maritime Register of Shipping: Saint-Petersburg, Russia, 2003. (In Russian)
10. Lopatoukhin, L.I.; Boukhanovsky, A.V.; Ivanov, S.V.; Chernysheva, E.S. *Reference Data of Wind and Waves Climate of the Baltic, North, Black, Azov and Mediterranean Seas*; Russian Maritime Register of Shipping: Saint-Petersburg, Russia, 2006; p. 450. (In Russian)
11. Lopatukhin, L.; Buhanovskij, A.; Chernyshova, E. *Reference Data on the Wind and Wave Regime of the Japan and Kara Seas*; Russian Maritime Register of Shipping: Saint-Petersburg, Russia, 2009; p. 356. (In Russian)
12. Lopatukhin, L.; Buhanovskij, A.; Chernyshova, E. *Reference Data of Wind and Waves Climate of the Bering and White Seas*; Russian Maritime Register of Shipping: Saint-Petersburg, Russia, 2010. (In Russian)
13. Sokolov, A.; Chubarenko, B. Temporal Variability of the Wind Wave Parameters in the Baltic Sea in 1979–2018 Based on the Numerical Modeling Results. *Phys. Oceanogr.* **2020**, *27*, 352–363. [[CrossRef](#)]
14. Yaitskaya, N. The Wave Climate of the Sea of Azov. *Water* **2022**, *14*, 555. [[CrossRef](#)]
15. Sharmar, V.; Markina, M. Evaluation of interdecadal trends in sea ice, surface winds and ocean waves in the Arctic in 1980–2019. *Russ. J. Earth Sci.* **2021**, *21*, ES2002. [[CrossRef](#)]
16. Cabral, I.S.; Young, I.R.; Toffoli, A. Long-Term and Seasonal Variability of Wind and Wave Extremes in the Arctic Ocean. *Front. Mar. Sci.* **2022**, *9*, 802022. [[CrossRef](#)]
17. Waseda, T.; Webb, A.; Sato, K.; Inoue, J.; Kohout, A.; Penrose, B. Correlated increase of high ocean waves and winds in the ice-free waters of the Arctic Ocean. *Sci. Rep.* **2018**, *8*, 4489. [[CrossRef](#)]

18. Liu, Q.; Babanin, A.; Zieger, S.; Young, I.; Guan, C. Wind and wave climate in the Arctic Ocean as observed by altimeters. *J. Clim.* **2016**, *29*, 7957–7975. [[CrossRef](#)]
19. Stopa, J.E.; Ardhuin, F.; Girard-Ardhuin, F. Wave climate in the Arctic 1992–2014: Seasonality and trends. *Cryosphere* **2016**, *10*, 1605–1629. [[CrossRef](#)]
20. Duan, C.; Dong, S.; Wang, Z. Wave climate analysis in the ice-free waters of Kara Sea Regio. *Stud. Mar. Sci.* **2019**, *30*, 100719. [[CrossRef](#)]
21. Aarnes, O.J.; Reistad, M.; Breivik, Ø.; Bitner-Gregersen, E.; Ingolf Eide, L.; Gramstad, O.; Magnusson, A.K.; Natvig, B.; Vanem, E. Projected changes in significant waveheight toward the end of the 21st century: Northeast Atlantic. *J. Geophys. Res. Ocean.* **2017**, *122*, 3394–3403. [[CrossRef](#)]
22. Akpınar, A.; Jafali, H.; Rusu, E. Temporal variation of the wave energy flux in hotspot areas of the Black Sea. *Sustainability* **2019**, *11*, 562. [[CrossRef](#)]
23. Divinsky, B.V.; Kosyan, R.D. Climatic trends in the fluctuations of wind waves power in the Black Sea. *Estuar. Coast. Shelf Sci.* **2020**, *235*, 106577. [[CrossRef](#)]
24. Onea, F.; Rusu, L. A Long-Term Assessment of the Black Sea Wave Climate. *Sustainability* **2017**, *9*, 1875. [[CrossRef](#)]
25. Aydoğan, B.; Ayat, B. Spatial variability of long-term trends of significant wave heights in the Black Sea. *Appl. Ocean. Res.* **2018**, *79*, 20–35. [[CrossRef](#)]
26. Alizadeh, M.J.; Nourani, V.; Kavianpour, M.R. A statistical framework to project wave climate and energy potential in the Caspian Sea: Application of CMIP6 scenarios. *Int. J. Environ. Sci. Technol.* **2022**, *19*, 2323–2336. [[CrossRef](#)]
27. Lopatoukhin, L.I.; Yaitskaya, N.A. Peculiarities of the Approach to Calculation of Wind Waves in the Caspian Sea. *Russ. Meteorol. Hydrol.* **2018**, *43*, 245–250. [[CrossRef](#)]
28. Lama, G.F.; Sadeghifar, C.; Azad, T.; Sihag, M.T.; Kisi, O. On the Indirect Estimation of Wind Wave Heights over the Southern Coasts of the Caspian Sea: A Comparative Analysis. *Water* **2022**, *14*, 843. [[CrossRef](#)]
29. Kudryavtseva, N.; Kussembayeva, K.; Rakisheva, Z.B.; Soomere, T. Spatial variations in the Caspian Sea wave climate in 2002–2013 from satellite altimetry. *Est. J. Earth Sci.* **2019**, *68*, 225–240. [[CrossRef](#)]
30. Kamranzad, B.; Etemad-Shahidi, A.; Chegini, V. Sustainability of wave energy resources in southern Caspian Sea. *Energy* **2016**, *97*, 549–559. [[CrossRef](#)]
31. Vrazhkin, A.N. Application of spectral wave model for some areas of the Far Eastern Seas and the Pacific Ocean. *Pac. Oceanogr.* **2013**, *6*, 5–9.
32. Lyubitskiy, Y.V.; Vrazhkin, A.N.; Kharlamov, P.O. Forecasting of hazardous marine hydrometeorological phenomena for the regions of oil and gas deposit development on the Sea of Okhotsk Shelf. *IOP Conf. Ser. Earth Environ. Sci.* **2021**, *895*, 012023. [[CrossRef](#)]
33. Iwasaki, S.; Otsuka, J. Evaluation of Wave-Ice Parameterization Models in WAVEWATCH III® Along the Coastal Area of the Sea of Okhotsk During Winter. *Front. Mar. Sci.* **2021**, *8*, 713784. [[CrossRef](#)]
34. Lee, H.S.; Kim, K.O.; Yamashita, T.; Komaguchi, T.; Mishima, T. Abnormal storm waves in the winter East/Japan Sea: Generation process and hindcasting using an atmosphere-wind wave modelling system. *Nat. Hazards Earth Syst. Sci.* **2010**, *10*, 773–792. [[CrossRef](#)]
35. Sasaki, W. Changes in wave energy resources around Japan. *Geophys. Res. Lett.* **2012**, *39*. [[CrossRef](#)]
36. Shimura, T.; Mori, N. High-resolution wave climate hindcast around Japan and its spectral representation. *Coast. Eng.* **2019**, *151*, 1–9. [[CrossRef](#)]
37. Berdnikov, S.V.; Dashkevich, L.V.; Kulygin, V.V.; Sheverdyayev, I.V.; Tretyakova, I.A.; Yaitskaya, N.A. EX-mare-forecasting system of natural hazards in the azov sea region. *Geogr. Environ. Sustain.* **2018**, *11*, 29–45. [[CrossRef](#)]
38. Myslenkov, S.A.; Medvedeva, A.Y. Wave energy resources of the Baltic Sea and coastal zone of the Kaliningrad Region. *Fundam. Appl. Hydrophys.* **2019**, *12*, 34–42. [[CrossRef](#)]
39. Soomere, T. Numerical simulations of wave climate in the Baltic Sea: A review. *Oceanologia* **2022**, *65*, 117–140. [[CrossRef](#)]
40. Arkhipkin, V.; Dobrolyubov, S.; Myslenkov, S.; Korablina, A. *The Wave Climate of the White Sea, Changing Climate and Socio-Economic Potential of the Russian Arctic*, 1st ed.; Sokratov, S., Ed.; Liga-Vent Moscow: Moscow, Russia, 2015; pp. 48–58.
41. Chernov, I.; Tolstikov, A. The White Sea: Available Data and Numerical Models. *Geosciences* **2020**, *10*, 463. [[CrossRef](#)]
42. Rivillas-Ospina, G.; Casas, D.; Maza, M.; Bolivar, M.; Ruiz, G.; Guerrero, R.; Horrillo-Caraballo, J.; Guerrero, M.; Diaz, K.; Rio, R.; et al. APPMAR 1.0: A Python application for downloading and analyzing of WAVEWATCH III® wave and wind data. *Comput. Geosci.* **2022**, *162*, 105098. [[CrossRef](#)]
43. Hemer, M.; Zieger, S.; Durrant, T.; O’Grady, J.; Hoeke, R.; McInnes, K.; Rosebrock, U. A revised assessment of Australia’s national wave energy resource. *Renew. Energy* **2016**, *114*, 85–107. [[CrossRef](#)]
44. Bingölbali, B.; Jafali, H.; Akpınar, A.; Bekiroğlu, S. Wave Energy Potential and Variability for the South West Coasts of the Black Sea: The WEB-based Wave Energy Atlas. *Renew. Energy* **2020**, *154*, 136–150. [[CrossRef](#)]
45. Arinaga, R.; Cheung, K.F. Atlas of global wave energy from 10 years of reanalysis and hindcast data. *Renew. Energy* **2012**, *39*, 49–64. [[CrossRef](#)]
46. Larsén, X.; Davis, N.; Hannesdóttir, Á.; Kelly, M.; Svenningsen, L.; Slot, R.; Imberger, M.; Olsen, B.; Floors, R. The Global Atlas for Siting Parameters project: Extreme wind, turbulence, and turbine classes. *Wind. Energy* **2022**, *25*, 1841–1859. [[CrossRef](#)]
47. Arctic Renewable Energy Atlas. Available online: <https://arcticrenewableenergy.org> (accessed on 18 April 2023).

48. Global Atlas for Renewable Energy. Available online: <https://www.irena.org/Energy-Transition/Project-Facilitation/Renewable-potential-assessment/Global-Atlas> (accessed on 18 April 2023).
49. National Renewable Energy Laboratory. Marine and Hydrokinetic Data. Available online: <https://maps.nrel.gov/marine-energy-atlas/> (accessed on 18 April 2023).
50. Ocean Energy Systems. Available online: <https://www.ocean-energy-systems.org/ocean-energy/gis-map-tool/> (accessed on 18 April 2023).
51. European Atlas of the Seas. Available online: https://ec.europa.eu/maritimeaffairs/atlas/maritime_atlas (accessed on 18 April 2023).
52. Gridasov, M.V.; Kiseleva, S.V.; Nefedova, L.V.; Popel', O.S.; Frid, S.E. Development of the geoinformation system "Renewable sources of Russia": Statement of the problem and choice of solution methods. *Therm. Eng.* **2011**, *58*, 924–931. [CrossRef]
53. Myslenkov, S.A.; Samsonov, T.E.; Kiseleva, S.V.; Arkhipkin, V.S.; Shestakova, A.A.; Umnov, P.M. Development of Web-Atlas of Available Wind and Wave Energy in the Coastal Zones of the Russian Seas: Information and Cartographic Support (on the Example of the Black Sea). *Altern. Energy Ecol. (ISJAEE)* **2018**, *16–18*, 39–54. [CrossRef]
54. Myslenkov, S.A.; Samsonov, T.E.; Shurygina, A.A.; Kiseleva, S.V.; Arkhipkin, V.S.; Shestakova, A.A.; Surkova, G.V.; Silvestrova, K.P.; Umnov, P.M. Development of Web-Atlas of Wind And Wave Available Energy in the Coastal Zones of the Russian Seas: Web Interface and Analytic Function. *Altern. Energy Ecol. (ISJAEE)* **2020**, *7–18*, 44–59. (In Russian)
55. Tolman, H. The WAVEWATCH III Development Group User Manual and System Documentation of WAVEWATCH III Version 6.07. Tech. Note 333, March 2019. NOAA/NWS/NCEP/MMAB 2019. Available online: https://www.researchgate.net/publication/336069899_User_manual_and_system_documentation_of_WAVEWATCH_III_R_version_607 (accessed on 18 April 2023).
56. Rogers, W.E.; Babanin, A.V.; Wang, D.W. Observation consistent input and whitecapping dissipation in a model for windgenerated surface waves: Description and simple calculations. *J. Atmos. Ocean. Technol.* **2012**, *29*, 1329–1346. [CrossRef]
57. Zieger, S.; Babanin, A.V.; Rogers, W.E.; Young, I.R. Observation-based source terms in the third-generation wave model WAVEWATCH. *Ocean Model.* **2015**, *96*, 2–25. [CrossRef]
58. Myslenkov, S.; Markina, M.; Arkhipkin, V.; Tilinina, N. Frequency of storms in the Barents Sea under modern climate conditions. *Vestn. Mosk. Univ. Seriya 5 Geogr.* **2019**, *2*, 45–54.
59. Myslenkov, S.; Platonov, V.; Kislov, A.; Silvestrova, K.; Medvedev, I. Thirty-Nine-Year Wave Hindcast, Storm Activity, and Probability Analysis of Storm Waves in the Kara Sea, Russia. *Water* **2021**, *13*, 648. [CrossRef]
60. Myslenkov, S.; Kruglova, E.; Medvedeva, A.; Silvestrova, K.; Arkhipkin, V.; Akpınar, A. Sergey Dobrolyubov Number of Storms in Several Russian Seas: Trends and Connection to Large-Scale Atmospheric Indices. *Russ. J. Earth Sci.* **2023**, *23*, ES000828.
61. Saha, S.; Moorthi, M.; Pan, H.L.; Wu, X.; Wang, J.; Nadiga, S.; Tripp, P.; Kistler, R.; Woollen, J.; Behringer, D.; et al. The NCEP climate forecast system reanalysis. *Bull. Am. Meteorol. Soc.* **2010**, *91*, 1015–1057. [CrossRef]
62. Saha, S.; Moorthi, S.; Wu, X.; Wang, J.; Nadiga, S.; Tripp, P.; Becker, E. The NCEP Climate Forecast System Version 2. *J. Clim.* **2014**, *27*, 2185–2208. [CrossRef]
63. Zijlema, M. Computation of wind-wave spectra in coastal waters with SWAN on unstructured grids. *Coast. Eng.* **2010**, *57*, 267–277. [CrossRef]
64. Abdolali, A.; Pringle, W.; Roland, A.; Mehra, A. Assessment of global wave models on unstructured domains. *Authorea* **2020**. [CrossRef]
65. Medvedeva, A.; Myslenkov, S.; Medvedev, I.; Arkhipkin, V.; Krechik, V.; Dobrolyubov, S. Numerical Modeling of the Wind Waves in the Baltic Sea using the Rectangular and Unstructured Grids and the Reanalysis NCEP/CFSR. *Proc. Hydrometeorol. Res. Cent. Russ. Fed.* **2016**, *362*, 37–54. (In Russian with English Summary)
66. Myslenkov, S.; Arkhipkin, V.; Koltermann, K.P. Evaluation of swell height in the Barents and White Seas. Moscow University Bulletin. Series 5. *Geography* **2015**, *5*, 59–66.
67. Myslenkov, S.; Shestakova, A.; Chechin, D. The impact of sea waves on turbulent heat fluxes in the Barents Sea according to numerical modeling. *Atmos. Chem. Phys.* **2021**, *21*, 5575–5595. [CrossRef]
68. Pavlova, A.; Myslenkov, S.; Arkhipkin, V.; Surkova, G. Storm Surges and Extreme Wind Waves in the Caspian Sea in the Present and Future Climate. *Civ. Eng. J.* **2022**, *8*, 1–31. [CrossRef]
69. Gippius, F.N.; Myslenkov, S.A. Black Sea wind wave climate with a focus on coastal regions. *Ocean. Eng.* **2020**, *218*, 108199. [CrossRef]
70. Myslenkov, S.A. Modeling of the wind waves in the Laptev, East Siberian and Chukchi seas. *Hydrometeorol. Res. Forecast.* **2023**, *1*, 87–101. [CrossRef]
71. Peucker, T.K.; Fowler, R.J.; Little, J.J.; Mark, D.M. *Digital Representation of Three-Dimensional Surfaces by Triangulated Irregular Networks (TIN)*; Technical Report No. 10; Department of Geography, Simon Fraser University: Burnaby, BC, Canada, 1976.
72. Baumann, P.; Hirschorn, E.; Masó, J. OGC Coverage Implementation Schema. Open Geospatial Consortium. 2017. Available online: <https://docs.ogc.org/is/09-146r6/09-146r6.html> (accessed on 22 May 2023).
73. Hengl, T. Finding the right pixel size. *Comput. Geosci.* **2006**, *32*, 1283–1298. [CrossRef]
74. Hersbach, H.; Bell, B.; Berrisford, P.; Biavati, G.; Horányi, A.; Muñoz Sabater, J.; Nicolas, J.; Peubey, C.; Radu, R.; Rozum, I.; et al. ERA5 Hourly Data on Single Levels from 1940 to Present. Copernicus Climate Change Service (C3S) Climate Data Store (CDS). 2023. Available online: <https://doi.org/10.24381/cds.adbb2d47> (accessed on 10 March 2023).

75. Roh, M.; Oh, S.-M.; Chang, P.-H.; Kang, H.-S.; Kim, H.-S. Sensitivity Analysis of Forecasting Performance for ST6 Parameterization in High-Resolution Wave Model Based on WAVEWATCH III. *J. Mar. Sci. Eng.* **2023**, *11*, 1038. [[CrossRef](#)]
76. Soran, M.; Amarouche, K.; Akpınar, A. Spatial calibration of WAVEWATCH III model against satellite observations using different input and dissipation parameterizations in the Black Sea. *Ocean. Eng.* **2022**, *257*, 111627. [[CrossRef](#)]

Disclaimer/Publisher's Note: The statements, opinions and data contained in all publications are solely those of the individual author(s) and contributor(s) and not of MDPI and/or the editor(s). MDPI and/or the editor(s) disclaim responsibility for any injury to people or property resulting from any ideas, methods, instructions or products referred to in the content.